Space Weather

RESEARCH ARTICLE
10.1029/2022SW003369

# Deep Electron Density Depletion Near Sunset Terminator on St. Patrick's Day Storm and Its Impacts on Skywave Propagation

**M. Ankita[1], S. Tulasi Ram[1], K. K. Ajith[2], and S. Sripathi[1]**

[1]Indian Institute of Geomagnetism, Navi Mumbai, India, [2]National Atmospheric Research Laboratory, Gadanki, India

**Key Points:**

- A deep electron density depletion occurred over a narrow longitude sector near sunset terminator due to large equatorial vertical drift
- The depletion caused severe limitations on the usable high frequency spectrum of Skywave communication systems by reducing the maximum usable frequency by more than 50%
- The depletion also resulted in a wide area of skip zones over equatorial regions where Skywave communication signals cannot be received

**Correspondence to:**

S. Tulasi Ram,
tulasiram.s@iigm.res.in

**Citation:**

Ankita, M., Tulasi Ram, S., Ajith, K. K., & Sripathi, S. (2023). Deep electron density depletion near sunset terminator on St. Patrick's Day storm and its impacts on Skywave propagation. *Space Weather*, *21*, e2022SW003369. https://doi.org/10.1029/2022SW003369

Received 5 DEC 2022
Accepted 12 FEB 2023

**Author Contributions:**

**Conceptualization:** S. Tulasi Ram
**Data curation:** K. K. Ajith
**Formal analysis:** M. Ankita, K. K. Ajith
**Investigation:** M. Ankita, S. Tulasi Ram
**Methodology:** M. Ankita, S. Tulasi Ram, S. Sripathi
**Project Administration:** S. Tulasi Ram, S. Sripathi
**Resources:** S. Tulasi Ram
**Software:** M. Ankita, K. K. Ajith
**Supervision:** S. Tulasi Ram
**Validation:** M. Ankita, K. K. Ajith, S. Sripathi
**Visualization:** M. Ankita, K. K. Ajith, S. Sripathi
**Writing – original draft:** M. Ankita, S. Tulasi Ram



**Abstract** The plasma density distribution in the equatorial and low latitude ionosphere can often be severely disturbed during active space weather events that can have paramount impacts on the long-distance high frequency (HF) radio wave (Skywave) communications through the ionosphere. On the St. Patrick's Day storm of 17 March 2015, a deep depletion of plasma with more than two orders of magnitude was observed over a narrow longitudinal sector near the sunset terminator. The controlled SAMI2 (Sami2 is Another Model of the Ionosphere) simulations indicate that a large equatorial vertical drift around sunset terminator can produce such a deep electron density depletion and strong reinforcement of equatorial ionization anomaly. The impacts of these ionospheric density disturbances on the Skywave communication systems have been investigated using an HF propagation simulator that solves the propagation path of radio waves under given background ionospheric conditions. The results clearly demonstrate that the usable HF spectrum for Skywave communications is reduced by more than 50% over the region of depletion. Further, large areas of skip zones, where the Skywave signals are not receivable, are produced due to low ionospheric densities over this region. This study can have important applications in the planning and operation of Skywave systems during the active space weather periods.

**Plain Language Summary** Earth's ionosphere acts as a mirror in space that reflects back the radio waves to the ground and facilitates Radio communication links over very far distances beyond the horizon. However, the ionosphere which is primarily produced via photo-ionization by solar radiations can often be greatly disturbed due to highly energetic events on the sun such as solar flares, Coronal Mass Ejection, etc., and the resultant changes in the Earth's near space. These ionospheric disturbances can have significant impacts on the usable radio wave spectrum and ground coverage area of reception for Skywave communication systems. This study investigates a unique event of deep ionospheric density depletion that occurred during the geomagnetic storm and its impacts on Skywave systems over equatorial and low latitude regions. This study provides important insights about the space weather impacts on long-distance radio communications and can have potential applications in the planning and operation of Skywave communication systems.

## 1. Introduction

During the active space weather periods, the transfer of solar wind energy and momentum to Earth's magnetosphere-ionosphere system leads to a variety of neutral and electrodynamical processes causing severe disturbances in the ionosphere. The equatorial Ionosphere is one of the most vulnerable regions that exhibit dramatic changes in electron density distribution during this period. During geomagnetic storms, the particle and joule heating at high latitudes drives a global scale thermospheric wind dynamo, generally known as Ionospheric Disturbance Dynamo (IDD) (Blanc & Richmond, 1980). Further, the high latitude region 1 and region 2 field-aligned currents also induce strong convection and overshielding electric fields which penetrates promptly to the equatorial ionosphere, known as Prompt Penetration Electric Field (PPEF) (Kikuchi et al., 1996, 2000; Nishida, 1968). The electric field perturbation associated with the above processes (IDD, strong convection, and overshielding electric fields) as well as neutral disturbances can significantly alter the electron density distribution of equatorial and low latitude ionosphere (Balan et al., 2012; Mannucci et al., 2005; Tulasi Ram et al., 2008, 2010).

Ionosphere is a medium that can significantly impact the propagation of radio waves due to the variation in radio refractive index which is directly dependent on ionospheric electron density. Several radio-communication applications such as long-distance high frequency (HF) communications (Skywave propagation) and over the

**Writing – review & editing:** M. Ankita, K. K. Ajith, S. Sripathi

horizon detection systems, use the ionosphere to reflect back radio waves in the HF band. Despite the growth of satellite based communications, the use of HF spectrum is also growing for both civilian and defense applications. In particular, HF communications become more important in rescue operations during natural disasters such as earthquakes, landslides, floods, etc. where the usual communication channels such as telephones and cellular communication become inaccessible. Any significant disturbances in the ionospheric electron density can have adverse impacts on these systems leading to loss of communication (Kelly et al., 2014). Further, the trans-ionospheric radio links between ground and satellite are also highly vulnerable to ionospheric disturbances which can lead to severe outages in satellite communications and GPS (Global Positioning System)-based augmentation systems during disturbed space weather events (Rama Rao et al., 2005, 2009).

A strong geomagnetic storm occurred on 17 March 2015 due to a Coronal Mass Ejection (CME) from the sun which hit the Earth's magnetosphere at ∼0430 UT (Kamide & Kusano, 2015). Subsequently, a geomagnetic storm developed with SYM-H reaching approximately −232 nT and is popularly known as St. Patrick's Day storm. Several interesting studies on the changes in the magnetosphere-ionosphere system have been reported in the literature (Astafyeva et al., 2015; Patra et al., 2016; Ramsingh et al., 2015; Tulasi Ram et al., 2016, 2019; Venkatesh et al., 2017). Astafyeva et al. (2015) have reported strong ionospheric disturbances using several ground and space-borne observations over American and European sectors. Ramsingh et al. (2015) have shown that the vertical drift at the Indian equatorial station Tirunelveli reached as large as 70 m/s during post-sunset hours which led to a strong spread F over the Indian sector. Tulasi Ram et al. (2016) have reported a uniquely enhanced convection electric field effects near the dusk terminator even under IDD effects prevailing in the background. Patra et al. (2016) have shown the occurrence of strong ESF echoes at very high altitudes (Field-Aligned Irregularities) that are uniquely confined to the Indian sector. Venkatesh et al. (2017) and Tulasi Ram et al. (2019) have also studied the ionospheric responses over the Brazilian and Indian sectors and demonstrated rapid intensification of Equatorial Ionization Anomaly (EIA) due to strong eastward penetration electric fields at the equator.

Tulasi Ram et al. (2016) have also reported a deep electron density depletion near sunset terminator using in situ ion density measurements from a low inclination orbiting satellite C/NOFS (Figure 4d of Tulasi Ram et al., 2016). They have speculated that the strong depletion at the sunset terminator is mainly due to the large vertical drift owing to the enhanced PPEF effects that uplifted the equatorial ionosphere to altitudes above the satellite orbit. In the current study, we further examine the effects of large vertical drifts on the re-distribution of equatorial ionospheric plasma near the sunset terminator using SAMI2 model simulations. Further, the impacts of such severe modifications in the electron density distribution on the Skywave radio propagation have been evaluated using an HF radio wave propagation simulator that solves the ray equations in three-dimensional space.

## 2. Data and Methodology

In this study, the solar wind parameters such as solar wind velocity, density, IMF $B_z$, and geomagnetic storm index (SYM-H) at 1-min time resolution from the OMNI-Web interface of NASA's Space Physics Data Facility (SPDF) (https://omniweb.gsfc.nasa.gov/form/omni_min.html) were considered to study the geomagnetic storm that occurred on 17 March 2015. The in situ ion density measurements from the Ion Velocity Meter (IVM) onboard the C/NOFS (Communications/Navigation Outage Forecasting System) satellite were used to study the longitudinal variations of ion density over equatorial and low latitudes (https://cdaweb.gsfc.nasa.gov/pub/data/cnofs/cindi/ivm_500ms_hdf/Daily_HDF/2015/). Further, the SAMI2 (Sami2 is Another Model of the Ionosphere) model has been employed to simulate and study the three-dimensional ionospheric electron density distribution and/or disturbances in response to the PPEF disturbances during the St. Patrick's Day storm. SAMI2 is a physics-based ionosphere model that solves the momentum and continuity equations of seven ion species in a grid of magnetic field lines and altitudes (Huba et al., 2000). To evaluate the impacts of the ionospheric disturbances on Skywave communication systems, an HF Radio wave propagation simulator was developed as briefly described in the below section.

### 2.1. HF Radio Wave Propagation Simulator

An HF propagation simulator is developed by solving the ray equations that give the radio wave position and direction vectors in a medium with inhomogeneously varying refractive index as given by Haselgrove (1954, 1963).

$$\dot{\mathbf{r}} = -\frac{\partial H}{\partial \boldsymbol{k}} \Big/ \frac{\partial H}{\partial \omega} \tag{1}$$

$$\dot{\mathbf{k}} = \frac{\partial H}{\partial \boldsymbol{r}} \Big/ \frac{\partial H}{\partial \omega} \tag{2}$$

The Hamiltonian required to solve these equations can be derived from the dispersion relation. There are many choices available from which Hamiltonian can be chosen. In this study, we are using Appleton Hartree Hamiltonian (Jones & Stephenson, 1975) which is given as

$$H = Re\left[\frac{c^2}{\omega^2}\left(k_x^2 + k_y^2 + k_z^2\right) - n^2\right] \tag{3}$$

Here, $k_x$, $k_y$, and $k_z$ are wave vectors in the $x$, $y$, and $z$ direction, and $n$ is the refractive index given by Appleton Hartree equation (Budden, 1988)

$$n^2 = 1 - \frac{X}{1 - iZ - \frac{\mathrm{Y}^2 \sin^2\theta}{2(1-X-iZ)} \pm \sqrt{\frac{\mathrm{Y}^4 \sin^4\theta}{4(1-X-iZ)^2} + \mathrm{Y}^2\cos^2\theta}} \tag{4}$$

$$X = \frac{Ne^2}{\varepsilon_0 m\omega^2}, \mathrm{Y} = \frac{|e|B}{m\omega}, Z = \frac{\nu}{\omega} \tag{5}$$

The above ray equations form six coupled ordinary differential equations that are numerically solved using the Cash-Karp integration method (Cash & Karp, 1990) at regular time intervals with a step size of 0.3 μs. At the end of each time step, the simulator computes the next position and direction of the wave and by doing so iteratively whole path traveled by the radio wave can be traced under given background ionospheric conditions.

This HF propagation simulator is thoroughly validated by comparing with ground-based Digisonde observations. For example, Figure 1 shows an Ionogram from a Digisonde at the Millstone hill station. The Digisonde system uses ARTIST 5 (Automatic Real-Time Ionogram Scaler with True height) (Galkin et al., 2008) software which automatically scales the Ionogram and computes the True height electron density profile (black curve). We now use this True height electron density profile as the background ionospheric density to derive propagation paths of radio waves that are vertically transmitted from the ground. The paths of both Ordinary (O mode) and Extraordinary (X mode) modes of propagation are traced at different frequencies up to the critical frequency. By computing the total time taken by the radio waves to reflect back to the ground, the virtual heights of reflection points are derived and virtual height curves are obtained. The blue and orange dashed curves in Figure 1 show the derived virtual height curves for O and X modes of propagation respectively. It can be seen from this figure that the derived virtual height curves of both O and X modes match very closely with the virtual height traces of the Digisonde Ionogram. This clearly demonstrates the accuracy of the HF radio wave simulator in predicting the path of radio waves under the given ionospheric electron density distribution. We use this simulator in later section (Section 3.2) to study the impacts of highly disturbed ionospheric conditions on Skywave communications during the St. Patrick's Day storm.

## 3. Results and Discussion

The strongest geomagnetic storm of solar cycle 24 that occurred on St. Patrick's Day (17 March 2015) is presented in Figure 2 which shows the temporal variations of solar wind velocity, density, and the vertical component of the interplanetary magnetic field (IMF $B_z$) (Figures 2a–2c) and SYM-H index (Figure 2d). The arrival of CME shock can be noticed as a sudden enhancement in solar wind parameters at 0448 UT. The IMF $B_z$ (Figure 2c) which was initially northward, turned southward at 0600 UT causing the onset of the main phase of geomagnetic storm. The main phase lasted for several hours and reached a minimum of −232 nT (Figure 2d) around 2304 UT.

### 3.1. Deep Electron Density Depletions and SAMI2 Simulations

The event of interest in this study presented in Figure 3, occurred at 1326 UT when the Indian sector is around the dusk region. Figure 3a shows the path of low inclination (13.5°) orbiting satellite C/NOFS around 1326 UT (blue curve) on 17 March 2015. The black curve indicates the geomagnetic equator. The vertical dashed line indicates the location of the F region sunset terminator corresponding to 1326 UT. The C/NOFS path on the previously quiet day (16 March 2015) around the same UT is also shown in the figure (Pink curve). In Figure 3b is shown the longitudinal variations of in situ ion density measured from the IVM onboard the C/NOFS on 17 March 2015

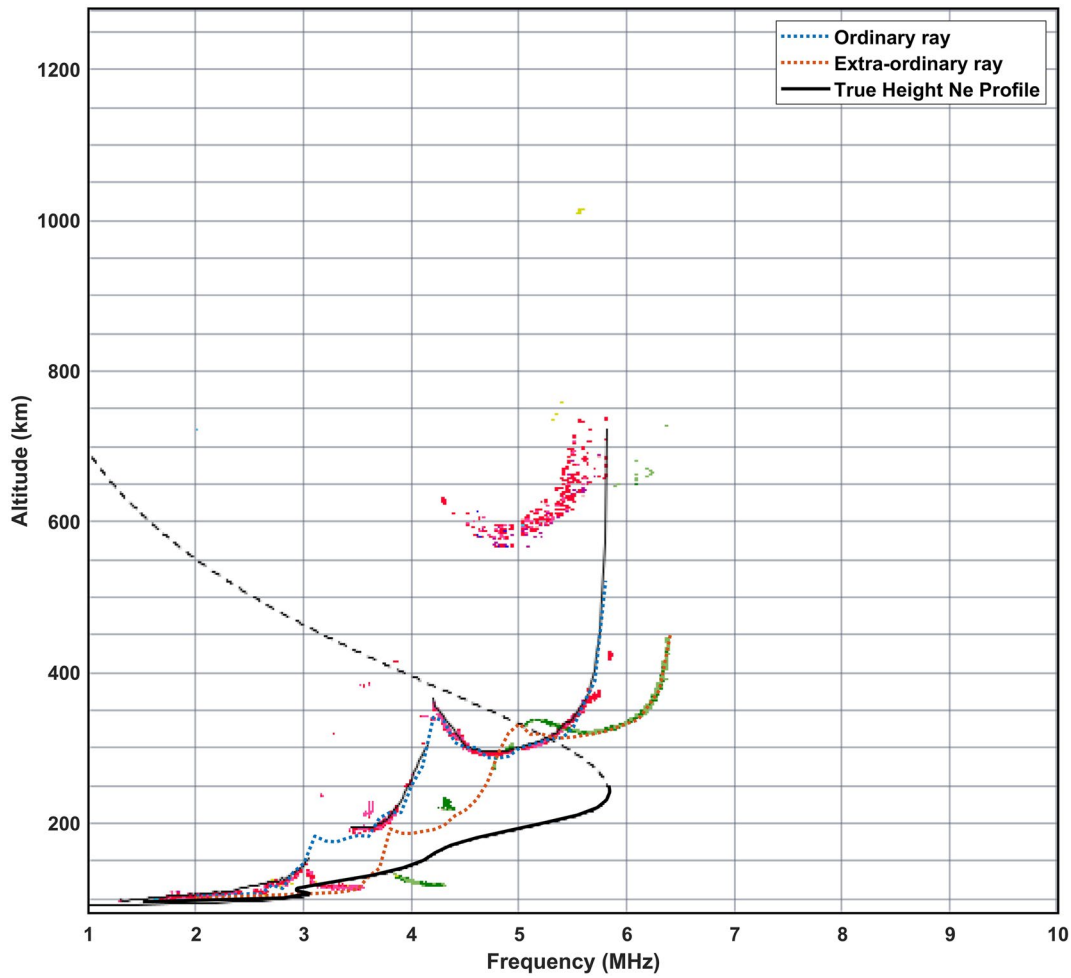


**Figure 1.** An example ionogram from a Digisonde at Millstone hill station. The thick black curve is the bottomside True Height electron density profile. The blue and orange dashed curves represent the virtual height traces for Ordinary and Extraordinary modes of propagation, respectively, computed from the HF radio wave propagation simulator.

around 1326 UT (blue curve). The ion density variation around the same UT and region on previously quiet day is also shown for reference (pink curve). It is very interesting to observe the in situ ion density measured by C/NOFS exhibits a deep depletion over a narrow longitudinal sector centered on the sunset terminator on the storm day. The ion density decreased very sharply and reduced by more than two orders of magnitude with reference to a few degrees west on the day side. Also, this depletion on the storm day is unusual and distinctly different compared to the previous quiet day.

Tulasi Ram et al. (2016) have attributed this depletion as due to the upliftment of the equatorial ionosphere to altitudes above the C/NOFS orbit. As a result, the in situ ion density observations from C/NOFS could detect very low ion density values over the longitudes near the dusk terminator. The strong upliftment in equatorial ionosphere has been attributed to enhanced eastward penetration electric field effect on the dusk sector that augments the usual post-sunset height rise (PSSR) due to pre-reversal enhancement. Evidently, a strong vertical drift of 70 m/s measured from ground-based Ionosonde observation at the Indian equatorial station Tirunelveli (77.7°E) is reported by Ramsingh et al. (2015) around the same time. The spread-F began to appear in ionograms over Indian sector only after 1350 UT (Ramsingh et al., 2015; Tulasi Ram et al., 2016). Thus the deep density depletion observed at 1326 UT is mainly due to the redistribution of equatorial plasma under strong eastward electric field and not due to a plasma bubble.

The deep electron density depletion resulted by strong vertical drift near the sunset terminator also causes steep gradients in the longitudinal direction as can be seen from Figure 3b. Further, such a strong vertical drift over

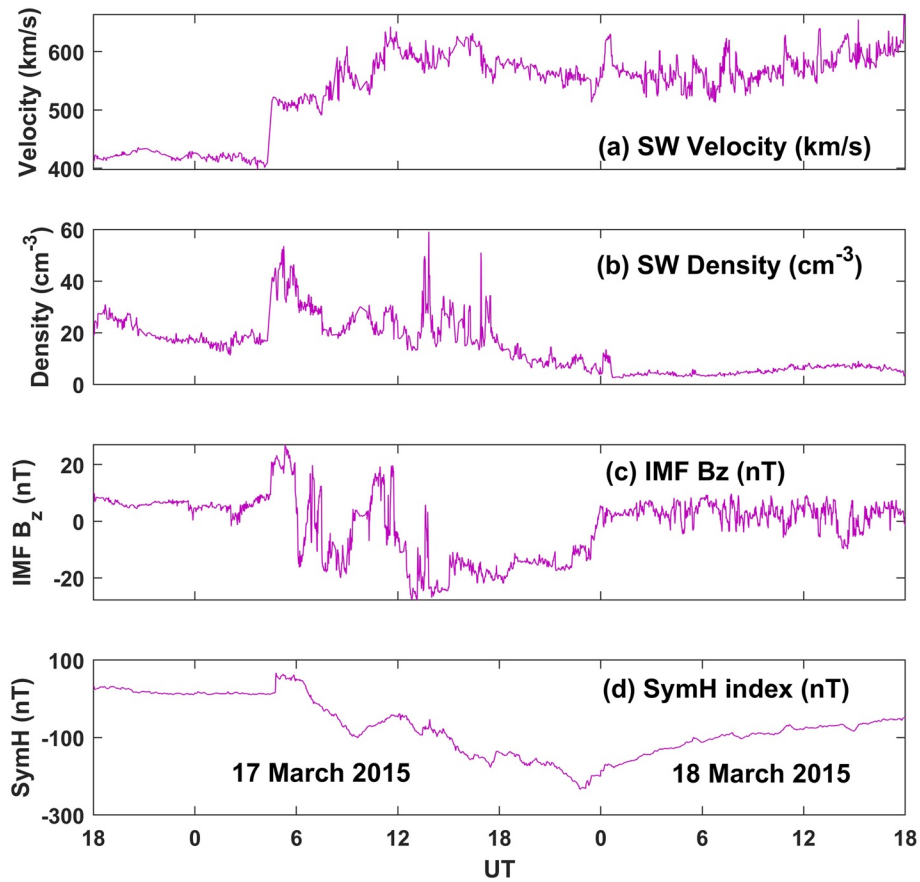


**Figure 2.** Universal time variations of (a) solar wind velocity, (b) density, (c) IMF $B_z$, and (d) SYM-H index during St. Patrick's day storm.

the equator is also expected to cause steep latitudinal gradients in the electron density due to rejuvenation of EIA via super fountain effect (Balan et al., 2009, 2012). Such significant modifications in the electron density distribution and spatial gradients in density can severely impact the radio communications in the HF band. With a view to examine the effects of such strong ionospheric disturbances over equatorial and low latitude regions and its impacts on the Skywave communication we have employed SAMI2 model to simulate a three-dimensional ionosphere reflecting such disturbances. SAMI2 uses Scherliess and Fejer model (Scherliess & Fejer, 1999) for vertical drift at the equator by default, although, it permits user-specified input of vertical drift for performing controlled model simulations. Figure 4 shows the electron density distribution simulated by SAMI2 model. The left-hand side panels represent latitude altitude distribution (Figure 4a) and longitude altitude distribution (Figure 4b) corresponding to quiet day conditions with default vertical drift values taken from the Scherliess and Fejer model (Figure 4c). The right-hand side panels (Figures 4d and 4e) show the electron density distribution by controlled SAMI2 simulation corresponding to the storm day. For this controlled simulation we have considered a maximum equatorial vertical drift of 70 m/s at 85°E longitude which gradually tapered down to smoothly connect with background vertical drift values at longitudes ±10° on either side as shown in Figure 4f. The other input parameters considered are, day number = 75, F10.7 = 116, Ap = 20 for quiet day and day number = 76, F10.7 = 113.20, Ap = 108 for storm day in the simulation. Distinct differences in the electron density distribution on the storm day due to the effects of strong vertical drift can be clearly observed compared to the quiet day. One of the most interesting observations that can be noted is a narrow tunnel like low density structure around 80°-90°E longitude in Figure 4e. The large vertical drift also resulted in a strong intensification of EIA with formation of broad trough region over the equator and dense crests departed significantly away from the equator (Figure 4d). The features observed in Figure 4e such as deep depletion over narrow longitude sector and Figure 4d the strong intensification of EIA can be attributed to PPEF effects that are enhanced near sunset terminator, as suggested by Abdu et al. (1998) and Tulasi Ram et al. (2016).

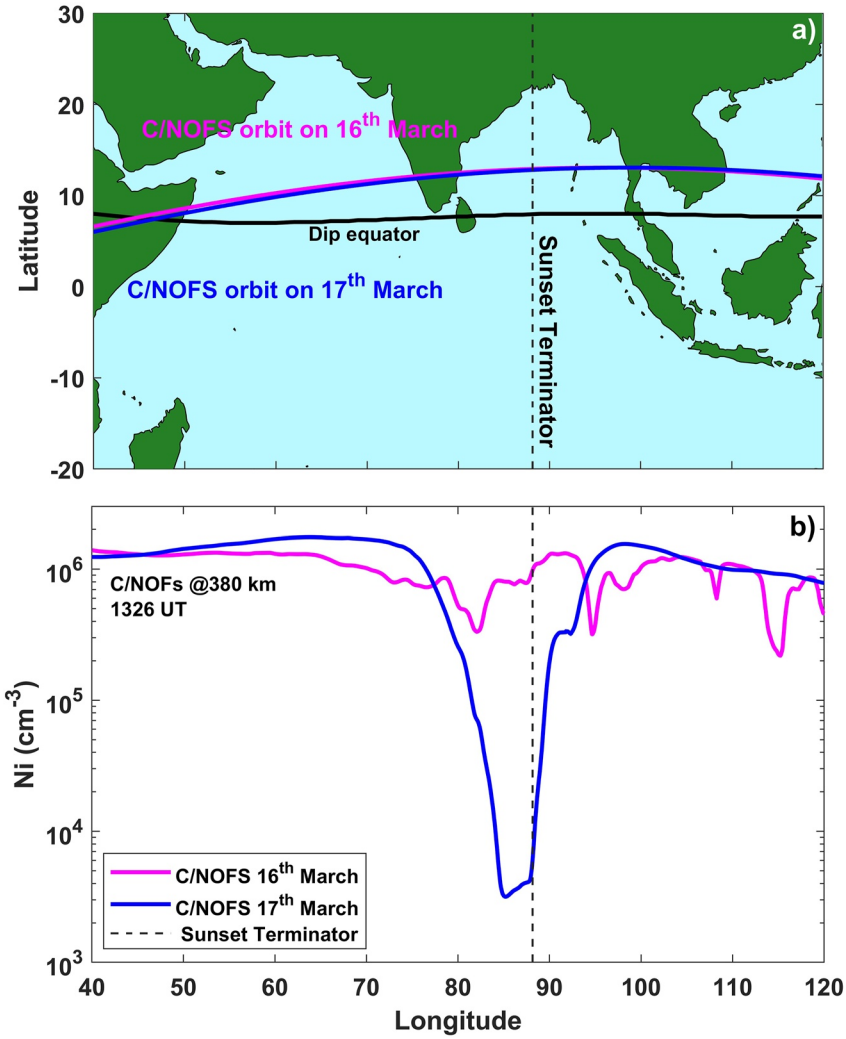


**Figure 3.** (a) Tracks of C/NOFS satellite passes on 16 March (Pink) and 17 March (Blue) 2015. The black curve represents the geomagnetic equator and the vertical dashed curves represents the location of F-region sunset terminator at 1326 UT (b) Shows the longitudinal variations of in situ ion density from C/NOFS on 16 March (Pink) and 17 March (Blue).

With a view to compare the SAMI2 simulated results with the in situ ion density measurements from C/NOFS (Figure 3b) the ion density variation along the exact path of C/NOFS has been obtained from the SAMI2 model simulated data and presented in Figure 5 (red curve). The in situ ion density measured by C/NOFS is also shown in the figure for comparison (blue curve). It is very interesting to note the SAMI2 simulated electron density reproduced a deep depletion over a narrow longitude sector similar to the in situ ion density measurements by C/NOFS. This result reconfirms that strong vertical drift near sunset terminator due to enhanced PPEF effects can induce such a deep depletion over a narrow longitude sector. It may also be noted that the depletion obtained from SAMI2 simulation is slightly smaller compared to the depletion in the C/NOFS in situ data. This difference in the magnitude of depletion can be due to the vertical drift of 70 m/s considered in the simulation based on the report of Ramsingh et al. (2015) from a slightly western Indian sector around 77.7°E longitude. The vertical drift at 85°E longitude might be larger than 70 m/s; however, we do not have any supporting observations about the exact vertical drift at 85°E longitude. In fact, the in situ vertical drift from IVM onboard the C/NOFS recorded a very large vertical drift of approximately 120 m/s around 85°E longitude (not show in figure). However, the sensitivity of IVM and ion drift values are unreliable under very low $O^+$ concentration levels (Stoneback et al., 2011). Hence, we have not considered ion drift values measured by C/NOFS in the present study. Another difference that can be observed in SAMI2 results is the decrease of density with an increase in longitude on the nightside, whereas the C/NOFS observation on the nightside is still at the same level as pre-sunset longitudes. This indicates

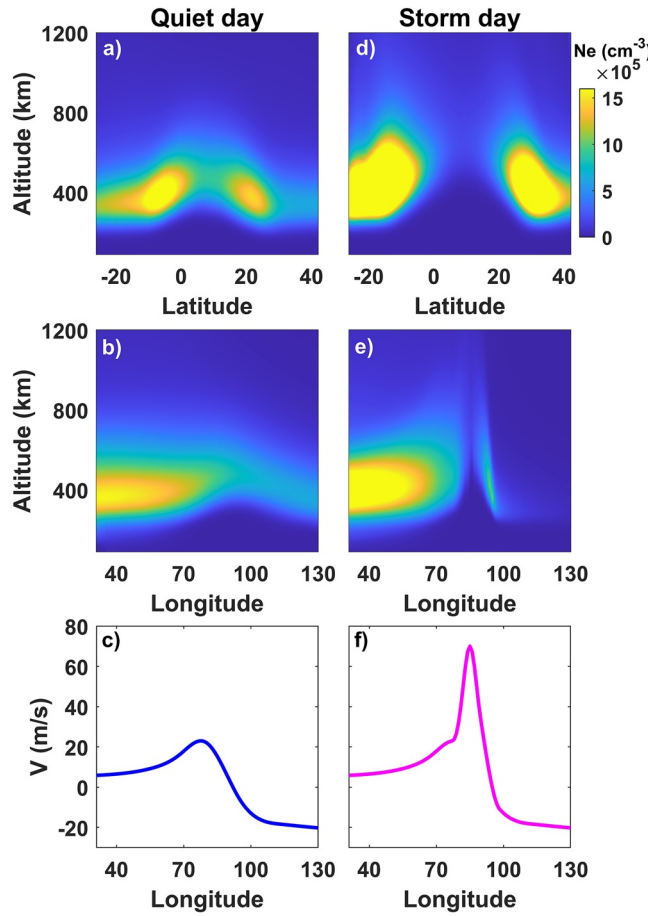


**Figure 4.** (top-panels) Latitude altitude distributions and (middle-panels) longitude altitude distribution of electron density simulated by SAMI2 model on quite (left side panels) and storm (right side panels) days. The bottom panels indicate the longitude variation of equatorial vertical drift used in SAMI2 simulations for quiet and storm days. For more details please refer text.

that the SAMI2 simulated data are more influenced by the recombination effects and westward electric fields after sunset. Inputting the actual plasma drift data from the eastern longitudes in the SAMI2 model could be helpful to minimize the differences between the C/NOFS observations and the model simulated results, however, we do not have vertical drift observations on the other longitude sectors. Although there are some differences in the magnitude of depletion and the night side electron density levels, the SAMI2 model simulation captured the steep depletion over narrow longitude around the sunset terminator reasonably well. It should be mentioned here that our purpose of employing SAMI2 simulation is not to exactly reproduce the electron density depletion observed by C/NOFS, but to generate nearly similar ionospheric conditions in order to evaluate its impacts on Skywave communication systems as discussed in the next section.

### 3.2. Impacts on Skywave Communications

Now the HF propagation simulator (described in Section 2.1) is used to evaluate the effects of strong equatorial ionospheric disturbances on the Skywave radio propagation systems. For this purpose, we use the SAMI2 model simulated three-dimensional electron density distributions of both quiet and storm days (Figure 4) as background ionospheric conditions in the simulator. For example, Figure 6 shows the longitude-altitude distribution of electron density simulated by SAMI2 on a quiet and storm day (same as Figures 4b and 4e). In Figures 6a and 6c radio waves of different frequencies are launched at 2 MHz interval from a transmitter located over the geomagnetic equator 8.7°N and 85°E (red star) at 60° elevation angle toward North (azimuth 90°). It can be seen from Figure 6a that on the quiet day the radio waves of lower frequencies 4–10 MHz are reflected back from the ionosphere and the 12 MHz wave escapes into the outer space. This defines the maximum usable frequency (MUF)

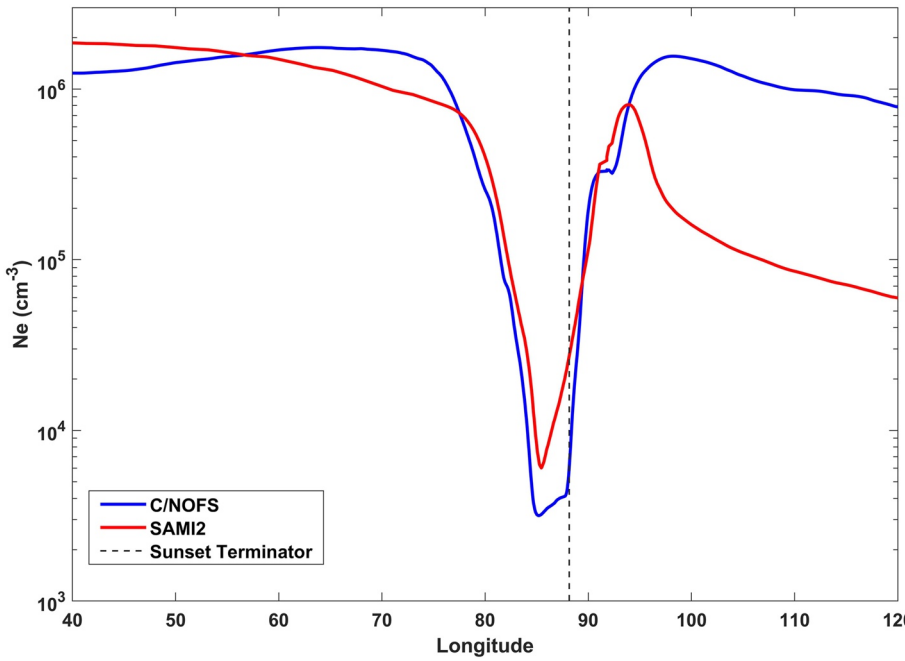


**Figure 5.** Comparison of ion density variation along the C/NOFS's pass simulated by SAMI2 (Red curve) with the actual in situ ion density measured by C/NOFS (Blue curve).

as 10 MHz for transmission in the direction with elevation 60° and azimuth 90° on the quiet day. However, due to the deep electron density depletion, the MUF on the storm day is reduced to 4 MHz (Figure 6c). In Figures 6b and 6d a radio wave of 10 MHz frequency is transmitted at different elevation angles at 10° intervals. The waves launched in the low elevation angles can be received at far distances on the ground. With increasing elevation angle the radio waves travel to much higher altitudes in the ionosphere and can escape to space after a critical elevation angle (50° in Figure 6b and 20° in Figure 6d). The ground distance of reception of radio wave at the critical elevation angle defines the minimum skip distance for Skywave communication for that given frequency. It can be seen from Figures 6b and 6d that the critical elevation angle has been decreased from 50° to 20° which resulted in significantly increased skip distance on the storm day.

Now we run the simulator at 0.1 MHz frequency resolution and transmit the signal in different directions by varying elevation and azimuth angles at regular intervals. This will give us the MUF distribution over a wide geographic area for transmissions from a given location. The location for the transmitter is chosen to coincide with the center of deep electron density depletion (8.7°N, 85°E). Figures 7a and 7b show the distribution of MUF for the quiet and storm days, respectively. The color-coded mesh grid shows the variation of MUF and the altitude of the mesh grid indicates the height from which the transmitted wave gets reflected back (reflection height). The contours below represent the ground projections of MUF corresponding to their point of reflection. One can clearly observe from these figures that MUFs on the storm day have been significantly reduced (more than 50%) compared to quiet day, particularly, at higher elevation angles. Further, on the storm day the transmitted radio waves penetrated to much higher altitudes before they get reflected back. The large reduction in MUF can severely affect communications at higher frequencies. Also, the higher reflection heights cause increased skip distances for transmissions at lower frequencies.

With a view to further examine the effects on the ground reception of Skywave signals, we have computed the first hop distances in different directions for different frequencies of transmission. Figure 8 shows the ground coverage of signal reception at their first hop distances during quiet (left-hand side panels) and storm (right-hand side panels) days. The color of contours represents the elevation angles. The unshaded area near the center of contours represents the minimum skip distance where the Skywave signal cannot be received. It can be seen from these figures (Figure 8) that the ground coverage of Skywave signal reception is severely distorted on the storm day, particularly, at higher frequencies. The low frequency signal such as 3 MHz (top panels) is received at all

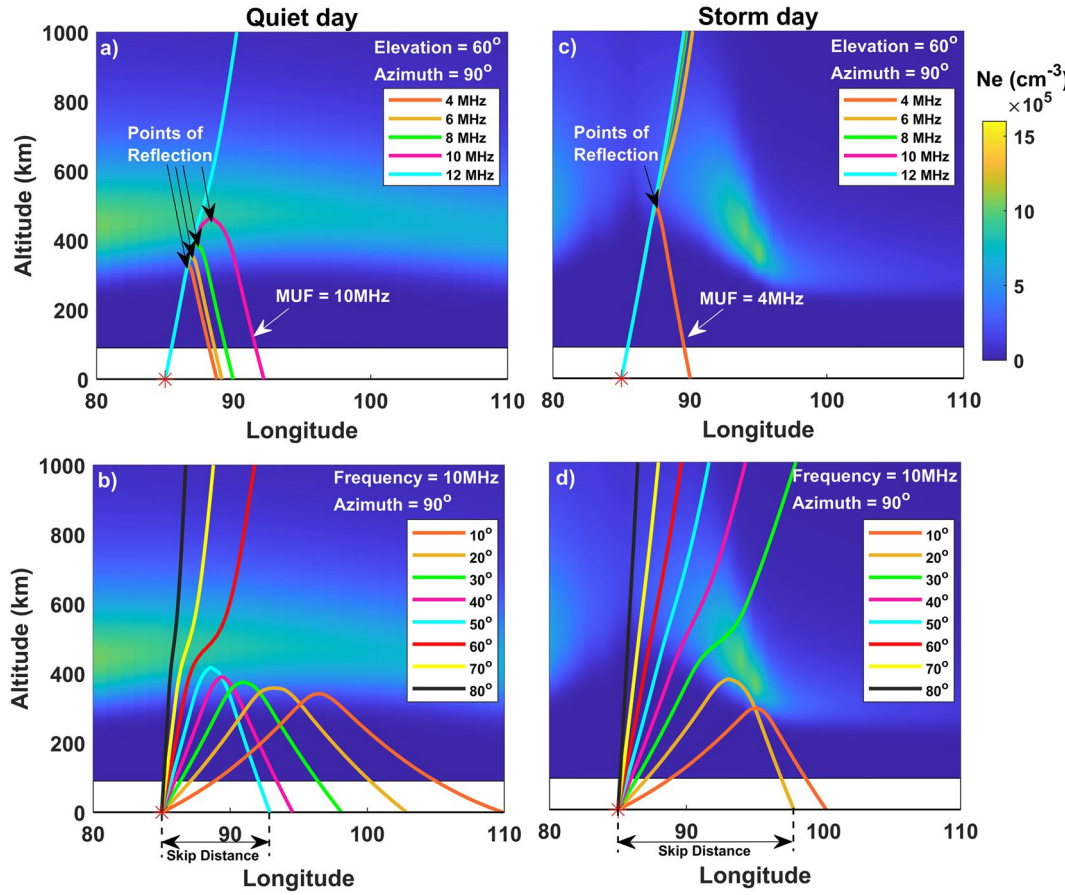


**Figure 6.** Illustration of radio wave propagation paths predicted by the simulator under the given ionospheric background conditions at different frequencies (top-panels) and elevation angles (bottom-panels) on quite (left side panels) and storm (right side panels) days. The definitions of MUFs, reflection heights and skip distances are as shown in the figure. Please refer text for more details.

elevation angles, however, the first hop distances of reception are higher on the storm day compared to the quiet day. This is mainly due to increased reflection heights as observed in Figure 7b. At higher frequencies a large area of skip zone is created near the center where the Skywave signals are totally lost. This is mainly due to the deep density depletion on the storm day allowing the high frequency signals to escape ionosphere at higher elevation angles. This is consistent with the reduced MUFs obtained on the storm day compared to the quiet day as seen from the simulation results presented in Figure 7. Therefore the results presented in Figures 7 and 8 clearly demonstrate that the deep electron density depletion observed on St. Patrick's Day storm can severely disturb the Skywave communications by creating large reductions in the MUFs and increased area of skip zones.

## 4. Summary

A deep electron density depletion over a narrow longitudinal sector centered on the sunset terminator has been observed by the C/NOFS satellite around 1326 UT near 85°E longitudinal sector on the St. Patrick's Day storm. The density near the center of depletion is smaller by nearly two orders of magnitude compared to few degrees on East and West of sunset terminator and exhibits sharp spatial gradients. Tulasi Ram et al. (2016) have suggested that the effects of PPEF can uniquely enhance near the dusk terminator causing the elevation of equatorial ionosphere to altitudes above the satellite orbit which results in such a deep depletion in the in situ measurements by C/NOFS. The strong equatorial vertical drifts of 70 m/s has also been reported by Ramsingh et al. (2015) from the Indian (77.7°E) sector. The disturbances in the equatorial ionospheric electron density distribution in response

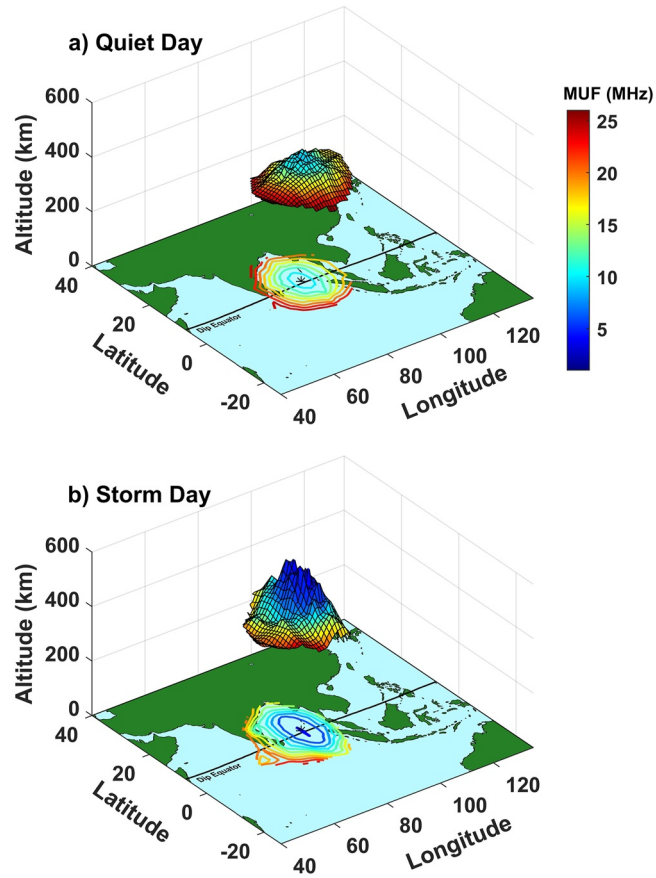


**Figure 7.** (a) Distributions of maximum usable frequencies under quiet and (b) disturbed ionospheric conditions on storm days. The color and the heights of the mesh grid represent the maximum usable frequency and the reflection heights respectively. The contours represent the ground projections of MUFs corresponding to the point of reflection.

to such a strong vertical drift have been simulated by the SAMI2 model with an input equatorial vertical drift of 70 m/s at 85°E longitude that gradually tapered to background levels on either side. Significant redistribution of equatorial plasma due to strong vertical drift is clearly evident from the SAMI2 simulation with a narrow depleted structure around 80°–90° longitudes (Figure 4e) and strong re-intensification of EIA (Figure 4d). Also, the model could successfully reproduce the deep density depletion over a narrow longitudinal sector that is nearly similar to that observed by C/NOFS around the dusk terminator (Figure 5). These results clearly portray the effects of enhanced PPEF near the sunset terminator on the equatorial and low-latitude ionospheric electron density distribution.

Further, the impacts of these ionospheric disturbances due to strong PPEF effects near the dusk terminator on the Skywave communications are studied using an HF radio wave propagation simulator that solves the position and direction of radio waves under the given ionospheric conditions (Section 2.1). The HF propagation simulator results clearly show that the reinforced EIA and deep electron density depletion near the sunset terminator can severely affect the Skywave communications over that region. The MUFs have been reduced by nearly 50% over the depleted region (Figure 7) causing severe limitations on the usable HF spectrum. Even at the lower segment of HF band, the radio waves propagated much higher altitudes in the ionosphere causing increased skip distances for the reception at ground. At higher frequencies, the transmitted radio waves mostly escape through ionosphere except at very low elevation angles (below 20°) thereby causing a large skip zone where the Skywave communication signals were totally lost (Figure 8). The area of skip zone increases with the increasing transmitted frequency and severely affects the Skywave communications over a large geographic area (Figure 8).

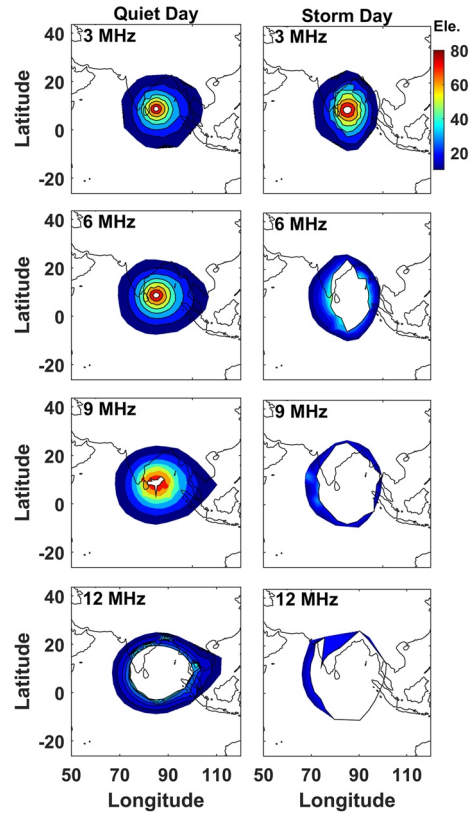


**Figure 8.** The ground coverage area of Skywave signal reception at their first hop distances for different frequencies. The color of the contour represents the elevation angle. The unshaded area near the center represents the area of skip zone.

This study showcases the impacts of space weather phenomena such as geomagnetic storm and enhanced PPEF near sunset terminator on the Skywave communication systems due to severe disturbances/modifications in the equatorial and low-latitude ionospheric electron density distribution. The results presented in this study would have potential applications in the planning and operation of long-distance and/or over-the-horizon HF communication systems during active space weather periods.

## Data Availability Statement

The solar wind and SYM-H index data is provided by NASA's SPDF and can be found through OMNI interface (https://omniweb.gsfc.nasa.gov/form/omni_min.html). The C/NOFS-IVM data are provided through the auspices of the CINDI team at the University of Texas at Dallas, supported by NASA Grant NAS5-01068 (https://cdaweb.gsfc.nasa.gov/pub/data/cnofs/cindi/ivm_500ms_hdf/Daily_HDF/2015/).

**Acknowledgments**
We acknowledge the open data policy of NASA's SPDF for the solar wind and SYM-H index data through OMNI interface. We also acknowledge CINDI team at the University of Texas at Dallas for providing C/NOFS-IVM data.

## References

Abdu, M. A., Sastri, J. H., Luhr, H., Tachihara, H., Kitamura, T., Trivedi, N. B., & Sobral, J. H. A. (1998). DP 2 electric field fluctuations in the dusk-time dip equatorial ionosphere. *Geophysical Research Letters*, *25*(9), 1511–1514. https://doi.org/10.1029/98GL01096

Astafyeva, E., Zakharenkova, I., & Förster, M. (2015). Ionospheric response to the 2015 St. Patrick's Day storm: A global multi-instrumental overview. *Journal of Geophysical Research: Space Physics*, *120*(10), 9023–9037. https://doi.org/10.1002/2015JA021629

Balan, N., Liu, J. Y., Otsuka, Y., Tulasi Ram, S., & Lühr, H. (2012). Ionospheric and thermospheric storms at equatorial latitudes observed by CHAMP, ROCSAT, and DMSP. *Journal of Geophysical Research*, *117*(A1), A01313. https://doi.org/10.1029/2011JA016903

Balan, N., Shiokawa, K., Otsuka, Y., Watanabe, S., & Bailey, G. J. (2009). Super plasma fountain and equatorial ionization anomaly during penetration electric field. *Journal of Geophysical Research*, *114*(A3), A03310. https://doi.org/10.1029/2008JA013768

Blanc, M., & Richmond, A. D. (1980). The ionospheric disturbance dynamo. *Journal of Geophysical Research*, *85*(A4), 1669–1688. https://doi.org/10.1029/JA085iA04p01669

Budden, K. G. (1988). *The propagation of radio waves: The theory of radio waves of low power in the ionosphere and magnetosphere*. Cambridge University Press.

Cash, J. R., & Karp, A. H. (1990). A variable order Runge-Kutta method for initial value problems with rapidly varying right-hand sides. *ACM Transactions on Mathematical Software*, *16*(3), 201–222. https://doi.org/10.1145/79505.79507

Galkin, I. A., Khmyrov, G. M., Kozlov, A. V., Reinisch, B. W., Huang, X., & Paznukhov, V. V. (2008). The ARTIST 5, in Radio sounding and plasma physics. *AIP Conference Proceedings*, *974*, 150–159. https://doi.org/10.1063/1.2885024

Haselgrove, J. (1954). Ray theory and a new method for ray tracing. In *Report of the Physical Society Conference on the Physics of the Ionosphere* (pp. 355–364). Cambridge University.

Haselgrove, J. (1963). The Hamiltonian ray path equations. *Journal of Atmospheric and Terrestrial Physics*, *25*(7), 397–399. https://doi.org/10.1016/0021-9169(63)90173-9

Huba, J. D., Joyce, G., & Fedder, J. A. (2000). Sami2 is Another Model of the Ionosphere (SAMI2): A new low-latitude ionosphere model. *Journal of Geophysical Research*, *105*(A10), 23035–23053. https://doi.org/10.1029/2000ja000035

Jones, R. M., & Stephenson, J. J. (1975). *A versatile three-dimensional ray tracing computer program for radio waves in the ionosphere* (Vol. 1). US Department of Commerce, Office of Telecommunications.

Kamide, Y., & Kusano, K. (2015). No major solar flares but the largest geomagnetic storm in the present solar cycle. *Space Weather*, *13*(6), 365–367. https://doi.org/10.1002/2015SW001213

Kelly, M. A., Comberiate, J. M., Miller, E. S., & Paxton, L. J. (2014). Progress toward forecasting of space weather effects on UHF SATCOM after Operation Anaconda. *Space Weather*, *12*(10), 601–611. https://doi.org/10.1002/2014SW001081

Kikuchi, T., Luhr, H., Schlegel, K., Tachihara, H., Shinohara, M., & Kitamura, T. L. (2000). Penetration of auroral electric fields to the equator during a substorm. *Journal of Geophysical Research*, *105*(A10), 23251–23261. https://doi.org/10.1029/2000JA900016

Kikuchi, T., Luhr, H., Kitamura, T., Saka, O., & Schlegel, K. (1996). Direct penetration of the polar electric fields to the equator during a DP 2 event as detected by the auroral and equatorial magnetometer chains and the EISCAT radar. *Journal of Geophysical Research*, *101*(A8), 17161–17173. https://doi.org/10.1029/96JA01299

Mannucci, A. J., Tsurutani, B. T., Iijima, B. A., Komjathy, A., Saito, A., Gonzalez, W. D., et al. (2005). Dayside global ionospheric response to the major interplanetary events of October 29–30, 2003 ‘‘Halloween Storms”. *Geophysical Research Letters*, *32*(12), L12S02. https://doi.org/10.1029/2004GL021467

Nishida, A. (1968). Coherence of geomagnetic DP 2 fluctuations with interplanetary magnetic variations. *Journal of Geophysical Research*, *73*(17), 5549–5559. https://doi.org/10.1029/JA073i017p05549

Patra, A. K., Chaitanya, P. P., Dashora, N., Sivakandan, M., & Taori, A. (2016). Highly localized unique electrodynamics and plasma irregularities linked with the 17 March 2015 severe magnetic storm observed using multi-technique common-volume observations from Gadanki, India. *Journal of Geophysical Research: Space Physics*, *121*(11), 11518–11527. https://doi.org/10.1002/2016JA023384

Rama Rao, P. V. S., Gopi Krishna, S., Vara Prasad, J., Prasad, S. N. V. S., Prasad, D. S. V. V. D., & Niranjan, K. (2009). Geomagnetic storm effects on GPS based navigation. *Annales Geophysicae*, *27*(5), 2101–2110. https://doi.org/10.5194/angeo-27-2101-2009

Rama Rao, P. V. S., Tulasi Ram, S., Niranjan, K., Prasad, D. D., Gopi Krishna, S., & Lakshmi, N. K. M. (2005). VHF and L-band scintillation characteristics over an Indian low latitude station, Waltair (17.7°N, 83.3°E). *Annales Geophysicae*, *23*(7), 2457–2464. https://doi.org/10.5194/angeo-23-2457-2005

Ramsingh, Sripathi, S., Sreekumar, S., Banola, S., Emperumal, K., Tiwari, P., & Kumar, B. S. (2015). Low-latitude ionosphere response to super geomagnetic storm of 17/18 March 2015: Results from a chain of ground based observations over Indian sector. *Journal of Geophysical Research: Space Physics*, *120*(12), 10864–10882. https://doi.org/10.1002/2015JA021509

Scherliess, L., & Fejer, B. G. (1999). Radar and satellite global equatorial F region vertical drift model. *Journal of Geophysical Research*, *104*(A4), 6829–6842. https://doi.org/10.1029/1999JA900025

Stoneback, R. A., Heelis, R. A., Burrell, A. G., Coley, W. R., Fejer, B. G., & Pacheco, E. (2011). Observations of quiet time vertical ion drift in the equatorial ionosphere during the solar minimum period of 2009. *Journal of Geophysical Research*, *116*(A12), A12327. https://doi.org/10.1029/2011JA016712

Tulasi Ram, S., Liu, C. H., & Su, S.-Y. (2010). Periodic solar wind forcing due to recurrent coronal holes during1996–2009 and its impact on Earth’s geomagnetic and ionospheric properties during the extreme solar minimum. *Journal of Geophysical Research*, *115*(A12), A12340. https://doi.org/10.1029/2010JA015800

Tulasi Ram, S., Nilam, B., Balan, N., Zhang, Q., Shiokawa, K., Chakrabarty, D., et al. (2019). Three different episodes of prompt equatorial electric field perturbations under steady southward IMF $B_z$ during St. Patrick's Day storm. *Journal of Geophysical Research: Space Physics*, *124*(12), 10428–10443. https://doi.org/10.1029/2019JA027069

Tulasi Ram, S., Rama Rao, P. V. S., Prasad, D. S. V. V. D., Niranjan, K., Gopi Krishna, S., Sridharan, R., & Ravindran, S. (2008). Local time dependent response of post sunset ESF during geomagnetic storms. *Journal of Geophysical Research*, *113*(A7), A07310. https://doi.org/10.1029/2007JA012922

Tulasi Ram, S., Yokoyama, T., Otsuka, Y., Shiokawa, K., Sripathi, S., Veenadhari, B., et al. (2016). Duskside enhancement of equatorial zonal electric field response to convection electric fields during the St. Patrick's Day storm on 17 March 2015. *Journal of Geophysical Research: Space Physics*, *121*(1), 538–548. https://doi.org/10.1002/2015JA021932

Venkatesh, K., Tulasi Ram, S., Fagundes, P. R., Seemala, G. K., & Batista, I. S. (2017). Electrodynamic disturbances in the Brazilian equatorial and low-latitude ionosphere on St. Patrick’s Day storm of 17 March 2015. *Journal of Geophysical Research: Space Physics*, *122*(4), 4553–4570. https://doi.org/10.1002/2017JA024009